RE-ENTRY RISK ASSESSMENT FOR LAUNCHERS – DEVELOPMENT OF THE NEW SCARAB 3.1L

T. Lips[1], B. Fritsche[1], M. Homeister[1], G. Koppenwallner[1], H. Klinkrad[2], and M. Toussaint[3]

[1]*HTG - Hypersonic Technology Göttingen, Max-Planck-Str. 19, 37191 Katlenburg-Lindau, Germany*
[2]*European Space Agency, ESA/ESOC, Robert-Bosch-Str. 5, 64293 Darmstadt, Germany*
[3]*European Space Agency, ESA/HQ, Rue Mario Nikis 8/10, 75015 Paris, France*

ABSTRACT

SCARAB (Spacecraft Atmospheric Re-Entry and Aerothermal Break-Up) is an ESA software tool allowing the analysis of mechanical and thermal destruction of spacecraft during controlled or uncontrolled re-entry. It is an integrated software package (flight dynamics, aerodynamics, aerothermodynamics, thermal and structural analysis) used to perform re-entry risk assessments (quantify, characterize and monitor surviving fragments during re-entry). The software has been validated with in-flight measurements and re-entry observations, and it has been compared to other re-entry prediction tools (NASA, FSA/Russia). The software has been developed continuously since 1995 and has evolved over time based on lessons learned from preceding software versions, upgrades and specific requests on re-entry analyses performed for various satellites (e.g. ROSAT, BeppoSAX, TerraSAR-X, GOCE), the Automated Transfer Vehicle (ATV), and the Ariane-5 launcher program. During the studies for the Ariane-5 stages, it turned out that the re-entry analysis of launch vehicle stages requires to model and to analyze special phenomena and features not necessary for satellites. Obvious differences to satellites are: tank bursting events due to the full or residual propellant loading, possibility of explosions due to fuel leaks or fuel release by tank bursting, different dynamic behavior due to sloshing effects. Consequently, the development of a special launcher dedicated extension – SCARAB 3.1L – started at the end of 2006. This extension intends to integrate into the latest SCARAB release all the complementary tools and analysis methods which have been developed due to urgent needs of launcher related re-entry analysis work in the last years. This paper describes the development history of SCARAB, the general analysis approach, and the implemented analysis methods, with special attention on the development of launcher specific analysis capabilities for the new SCARAB 3.1L.

1. INTRODUCTION

The development of SCARAB started in 1995 with an ESOC (European Space Operation Center) contract awarded to HTG with ITAM (Institute of Theoretical and Applied Mechanics, Russia), GMV (Grupo de Mecánica del Vuelo, Spain), and FGE (Fluid Gravity Engineering, United Kingdom) as subcontractors. This team established the basis for SCARAB. They combined five technical disciplines, aerodynamics, aerothermodynamics, dynamics, thermodynamics, and structural mechanics, which are relevant to perform a numerical re-entry simulation of a spacecraft including its destruction into one multi-disciplinary analysis system. The development of SCARAB 1.0 was completed end of 1997.[1]

Mid of 1998, shortly after the release of SCARAB 1.0, a new contract was awarded to HTG, ITAM, Energocosmos (Russia), and the Moscow State University for the development of SCARAB 2.0. The main objective for this development was to improve and optimize the first version in order to make SCARAB applicable to re-entry analyses for projects like Ariane-5 and ATV. The development of SCARAB 2.0 was completed early in the year 2000, with an additional contract extension completed in 2002.[2,3]

During the development of SCARAB 2.0, requests for comparisons between SCARAB and NASA's re-entry analysis software ORSAT (Object Reentry Survival Analysis Tool) came from the IADC (Inter-Agency Space Debris Coordination Committee). Furthermore, a re-entry analysis for ATV was requested by ESA. In order to accomplish these tasks, an intermediate upgrade of SCARAB 1.0 was necessary since SCARAB 2.0 was not yet available. This lead to the HTG in-house development of SCARAB 1.5.[4]

Although SCARAB 1.5 was never meant to be an official release of SCARAB, this version was later on also used for many other re-entry analyses like for ROSAT, Ariane-5 stages (EPC, EPS and ESC-A), BeppoSAX, TerraSAR-X, and GOCE. The decision to use SCARAB 1.5 instead of SCARAB 2.0, which was completed in the meantime, was mainly driven by its stable performance and the good confidence of the users in this version. Many additional features were developed to fulfill the analysis requests of the projects, all summarized in a support toolbox for SCARAB 1.5.

The disadvantage of the decision to keep on using SCARAB 1.5 for the requested re-entry analyses was that SCARAB 2.0 was never brought to similar maturity. Thus, some of the new desirable features of SCARAB 2.0 were not available for these analyses.

The development of SCARAB 3.0 started at the beginning of 2002. One of the main objectives for this version was to merge the two development branches. The capabilities of SCARAB 1.5 (incl. its support toolbox) and SCARAB 2.0 should be combined into one integrated version with project maturity. This goal was achieved by the end of 2005.[5] SCARAB 3.0 has just successfully completed its first application to an Ariane-5 EPC re-entry analysis.[6]

The complex studies for Ariane-5 stages performed in the past revealed that re-entry analyses for launch vehicle stage require additional or different analysis capabilities, respectively, than for satellite re-entries. Finally, this lead to the latest step in the SCARAB development history: SCARAB 3.1L ("L" for launcher). The development of this version started end of 2006 and should be completed until the end of 2008. The objective is to upgrade SCARAB 3.0 by implementing those analysis features which have been identified to be especially necessary for the analysis of launcher stage re-entries.

2. GENERAL ANALYSIS APPROACH

The SCARAB software distinguishes between two basic steps: spacecraft modeling and re-entry analysis. The modeling step comprises the complete geometry definition of the spacecraft based on geometric primitives (e.g. spheres, boxes, cylinders, etc.). The surface of each primitive is partitioned into triangular surface panels with user-defined resolution (see FIG. 1). These panels are the primary basis for all analysis steps. A material can be assigned to each primitive. The properties of these materials (e.g. density, melting temperature, heat capacity, etc.) are stored in SCARAB's material database. This material database provides constant and temperature dependent properties, and can be extended by the user depending on his modeling needs.

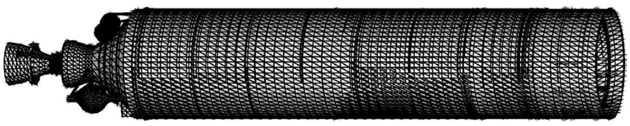

FIG. 1: Geometric SCARAB Model of Ariane-5 EPC (cryogenic main stage)

The re-entry analysis can be subdivided into three basic tasks: dynamic, thermal, and fragmentation analysis. The dynamic analysis provides the computation of the re-entry trajectory and the attitude motion of the spacecraft. The thermal analysis calculates the heating and melting of the spacecraft during re-entry. The fragmentation analysis determines the destruction of the spacecraft into fragments. All fragments can either demise completely, break-up into new fragments, or impact on the ground. All fragments must be subject to all three analysis tasks separately.

The dynamic analysis numerically solves the equation motion (Runge-Kutta method with variable time steps based on error estimations). The sums of all acting forces and torques form the right sides of the equations of motion. Eq. 1 is the force equation given in the inertial frame (superscript index I), Eq. 3 is the moment equation given in the body-fixed frame (superscript index B). The spacecraft position and attitude vectors are calculated by solving the differential Eqs. 2 and 4.

$$m_{SC}\,\dot{\vec{V}}^I = \sum_i \vec{F}_i^I(\vec{r}^I,\vec{q}^I,t) \tag{1}$$

$$\dot{\vec{r}}^I = \vec{V}^I \tag{2}$$

$$I\,\dot{\vec{\omega}}_{I,B}^B + \dot{I}\,\vec{\omega}_{I,B}^B + \vec{\omega}_{I,B}^B \times I\,\vec{\omega}_{I,B}^B = \sum_i \vec{T}_i^B(\vec{r}^I,\vec{q}^I,t) \tag{3}$$

$$\dot{\vec{q}}^I = 0.5\,Q\,\vec{\omega}_{I,B}^B \tag{4}$$

m_{SC}	Spacecraft mass
$\dot{\vec{V}}^I$	Spacecraft acceleration vector
$\vec{F}_i^I$	External force vectors
$\vec{r}^I$	Spacecraft position vector (center of mass)
$\vec{q}^I$	Quaternion vector (spacecraft attitude w.r.t. inertial frame)
t	Time
$\dot{\vec{r}}^I, \vec{V}^I$	Spacecraft velocity vector (center of mass)
I	Spacecraft moments of inertia matrix
$\dot{\vec{\omega}}_{I,B}^B$	Angular acceleration vector of the body-fixed axes w.r.t. inertial frame
$\dot{I}$	Time derivative of the spacecraft moments of inertia matrix
$\vec{\omega}_{I,B}^B$	Angular velocity vector of the body-fixed axes w.r.t. inertial frame
$\vec{T}_i^B$	External torque vectors
$\dot{\vec{q}}^I$	Time derivative of the quaternion vector
Q	Quaternion matrix of the spacecraft attitude in the inertial frame

The thermal analysis calculates the temperature of each panel of the geometry. Each panel has a uniform temperature (one thermal node). The panel temperatures are computed based on Eq. 5. The left side of this panel heat balance gives the sum of all heat sources and sinks, the right side gives the corresponding temperature change depending on the panel mass and the specific heat capacity of the panel material.

$$\dot{Q}_{p,tot} = \dot{Q}_{p,conv} + \dot{Q}_{p,cond} + \dot{Q}_{p,rad} = m_p\,c_p\,\frac{dT_p}{dt} \tag{5}$$

$\dot{Q}_{p,tot}$	Total heat flux on the panel
$\dot{Q}_{p,conv}$	Convective (aerothermodynamic) heat flux on the panel
$\dot{Q}_{p,cond}$	Conductive heat flux on the panel
$\dot{Q}_{p,rad}$	Radiative heat flux on the panel
m_p	Panel mass
c_p	Specific heat capacity of the panel material
T_p	Panel temperature

In SCARAB, the convective (aerothermodynamic) heat flux is always positive. Convective cooling is neglected as the aerodynamic and aerothermodynamic methods are only valid for hypersonic conditions ($Ma > 6$). The conductive heat flux summarizes the net heat flux (positive or negative) resulting from conductive heat exchange of a panel with all its neighbor panels. It depends on the temperature gradients between the thermal nodes and the thermal conductivity of the panel materials. The radiative heat flux computation considers by default only the radiative cooling and is therefore always negative. It depends on the panel temperature and the emission coefficient of the material. External radiative heating (e.g. from the shock in front of the spacecraft) is neglected as this is usually only relevant for high speed re-entries of spacecraft coming from outer space (e.g. planetary probe re-entries). Radiative heat exchange between panels is implemented in SCARAB but usually not used as the computation effort for this feature is very high.

The thermal analysis has to distinguish between panel heating and melting. If the melting temperature of a panel is reached, the panel temperature remains constant and the panel mass is reduced:

$$\dot{Q}_{p,tot} = -q_m \frac{dm_p}{dt} \tag{6}$$

q_m	Specific heat of melting of the panel material

The fragmentation analysis considers two effects: thermal and mechanical fragmentation. Thermal fragmentation is the separation of spacecraft components due to melting of connecting elements. A structural integrity check algorithm determines after each simulation time step if there are unconnected groups of panels. These fragments are treated as separate fragments afterward. Mechanical fragmentation means the breaking of connections due to acting forces and torques. Whereas thermal fragmentation is considered throughout the complete re-entry analysis, mechanical fragmentation is only determined for a limited number of user-defined cut planes. A cut plane through the spacecraft defines the load-bearing joints (group of panels intersected by the cut plane) and the two fragments on both sides of the cut plane. The stress inside the joints is calculated based on the forces and torques acting on the two spacecraft parts separated by the cut plane. If the stress exceeds the strength of the joint material (temperature dependent), the connection breaks and the two fragments are also treated as separate fragments.

3. ANALYSIS METHODS

3.1. Aerodynamics

Eqs. 1 and 3 require the sum of all forces and torques acting on the spacecraft during re-entry. By default, SCARAB considers loads from aerodynamics, gravitation (including zonal harmonic terms up to J8), third body perturbations (Sun and Moon), and solar radiation pressure. Since SCARAB 3.0, also forces and torques caused by thruster firings can be included.

The most complex analysis method is the aerodynamic analysis. The aerodynamics module of all SCARAB versions determines the aerodynamic loads depending on the actual flow conditions (free molecular, transition regime, continuum flow), spacecraft shape and attitude. This is achieved by an integration of the pressure and shear stress components acting on the unshadowed surface panels.

$$\vec{F}_A = 0.5\,\rho_\infty V_\infty^2 \int_{S_{us}} (c_p\,\vec{n} + c_\tau\,\vec{t})\, dS_{us} \tag{7}$$

$$\vec{M}_A = 0.5\,\rho_\infty V_\infty^2 \int_{S_{us}} [(\vec{r} - \vec{r}_{CM}) \times (c_p\,\vec{n} + c_\tau\,\vec{t})]\, dS_{us} \tag{8}$$

$\vec{F}_A$	Aerodynamic force vector
$\vec{M}_A$	Aerodynamic torque vector
ρ_∞	Free stream density
V_∞	Free stream velocity
c_p	Local pressure coefficient
c_τ	Local shear stress coefficient
$\vec{n}$	Panel normal vector
$\vec{t}$	Panel tangential vector
S_{us}	Unshadowed surface
$\vec{r}$	Panel position (center)
$\vec{r}_{CM}$	Spacecraft center of mass

Free molecular flow (subscript index FM):

$$\begin{aligned} c_{p,FM} = &\frac{1}{S_\infty^2}\left[\frac{\Pi(S_n)}{\sqrt{\pi}} + \frac{\chi(S_n)}{2}\sqrt{\frac{T_W}{T_\infty}}\right] \\ &+ \sqrt{\left(\frac{\Pi(S_n)}{\sqrt{\pi}\,S_\infty^2}\right)^2 + \left(\frac{\chi(S_n)}{\sqrt{\pi}\,S_\infty}\sin\theta\right)^2} \\ &\cdot \left(a_n + b_n\,\frac{2\,\theta}{\pi}\right) \end{aligned} \tag{9}$$

$$c_{\tau,FM} = \frac{\sin\theta}{\sqrt{\pi}\,S_\infty}\,\chi(S_n)\left(1 + a_t + b_t\left(\frac{2\,\theta}{\pi} - \frac{1}{2}\right)\right) \tag{10}$$

with:

$$\Pi(S_n) = S_n\,\mathrm{e}^{-S_n^2} + \sqrt{\pi}\left(S_n^2 + \frac{1}{2}\right)[1 + \mathrm{erf}(S_n)]$$

$$\chi(S_n) = \mathrm{e}^{-S_n^2} + \sqrt{\pi}\,S_n\,[1 + \mathrm{erf}(S_n)]$$

$$\mathrm{erf}(S_n) = \frac{2}{\sqrt{\pi}}\int_0^{S_n} \mathrm{e}^{-x^2}\,dx$$

$$S_n = S_\infty\cos\theta$$

$$S_\infty = Ma_\infty\sqrt{\kappa/2}$$

S_∞	Free stream speed ratio
S_n	Normal fraction of S_∞
T_W	Wall temperature
T_∞	Free stream temperature
θ	Local flow inclination (see FIG. 2)
a_n, b_n	Nocilla coefficients (normal)
a_t, b_t	Nocilla coefficients (tangential)
Ma_∞	Free stream Mach number
κ	Specific heats ratio

Continuum flow (subscript index C):

$$c_{p,C} = k_{N1}\,c_{p0}\cos^2\theta + k_{N2} \tag{11}$$

$$c_{\tau,C} = 0 \tag{12}$$

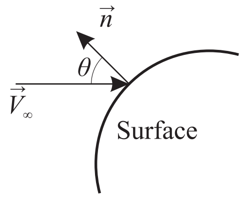

FIG. 2: Local Flow Inclination

with:

$$c_{p0} = \left(\frac{p_{st}}{p_\infty} - 1\right) \cdot \frac{2}{\kappa Ma_\infty^2}$$

$$\frac{p_{st}}{p_\infty} = \left(\frac{\kappa+1}{2} Ma_\infty^2\right)^{\frac{\kappa}{\kappa-1}} \cdot \left(\frac{\kappa+1}{2\kappa Ma_\infty^2 - \kappa + 1}\right)^{\frac{1}{\kappa-1}}$$

and correction factors k_{N1} and k_{N2} for modified Newtonian theory:

$\cos\theta \geq 0.73$: $\quad k_{N1} = 1 \quad k_{N2} = 0$
$\cos\theta \leq 0$: $\quad k_{N1} = 0 \quad k_{N2} = 0$
$0.73 > \cos\theta > 0$:

$$k_{N1} = 1 - \frac{0.73 - \cos\theta}{0.73}$$

$$k_{N2} = \frac{0.73 - \cos\theta}{0.73}\left[(\kappa+1)\cos^2\theta + \frac{4}{Ma_\infty^2(\kappa+1)}\right]$$

p_{st}	Stagnation point pressure
p_∞	Free stream pressure

Transitional regime:

(13) $$c_p = c_{p,C} + (c_{p,FM} - c_{p,C})\, f_p(Kn_p)$$

(14) $$c_\tau = c_{\tau,FM}\, f_\tau(Kn_\tau, \theta)$$

with bridging functions f_p and f_τ:

$$f_p = \frac{1}{2}\left(1 + \mathrm{erf}\left[\frac{\sqrt{\pi}}{\Delta Kn_p}\log\left(\frac{Kn_p}{1.8}\right)\right]\right)$$

$$Kn_p > 1.8: \qquad \Delta Kn_p = 1.3$$
$$Kn_p \leq 1.8: \qquad \Delta Kn_p = 1.4$$

$$f_\tau = \frac{1}{2}\left(1 + \mathrm{erf}\left[\frac{\sqrt{\pi}}{\Delta Kn_\tau}\log\left(\frac{Kn_\tau}{0.555}\right)\right]\right)$$

$$Kn_\tau > 0.555: \qquad \Delta Kn_\tau = 1.5$$
$$Kn_\tau \leq 0.555: \qquad \Delta Kn_\tau = 2.5$$

$$Kn_p = Kn_{\infty,0}$$

$$Kn_\tau = Kn_{\infty,0}/(0.2 + 0.8\cos^2\theta)$$

$$Kn_{\infty,0} = \lambda_{\infty,0}(\rho_\infty, T_0)/L_{ref}$$

$$\lambda_{\infty,0} = \frac{3.2 \cdot \mu(T_0)}{\rho_\infty\sqrt{\pi}\sqrt{2RT_0}}$$

$$L_{ref} = 2\sqrt{A_{pr}/\pi}$$

$Kn_{\infty,0}$	Modified Knudsen number
$\lambda_{\infty,0}$	Modified mean free path
T_0	Temperature behind normal shock
L_{ref}	Spacecraft reference length (diameter of a sphere with equivalent projected area)
μ	Dynamic viscosity
R	Gas constant
A_{pr}	Spacecraft projected area

3.2. Aerothermodynamics

The aerothermodynamics module of SCARAB calculates the convective heat flux $\dot{Q}_{p,conv}$ from the flow onto the surface panels of the modeled spacecraft, required by Eqs. 5 and 6. As for the aerodynamics analysis, the convective heat fluxes depend on the actual flow conditions (free molecular, transition regime, continuum flow), spacecraft shape and attitude.

In continuum flow, SCARAB 1.0 used the interpolation formula proposed by Detra, Kemp, and Riddell[7] for the stagnation point heat flux in laminar flow. The profile of the laminar heat transfer around the spacecraft was computed using a combination of the laminar stagnation value and tabular laminar heat transfer profiles for various blunt bodies (ellipsoids with different fineness ratios). For turbulent heat transfer, the local heat fluxes were directly computed based on the interpolation formula proposed by Detra and Hidalgo[8]. This approach provided the local turbulent heat transfer depending on the distance from the stagnation point, which was approximated by the shortest distance between the surface position and the stagnation point. The choice of whether to use the laminar or turbulent formulations was made using a standard Reynolds number approach.

In free-molecular flow, the local heat fluxes on the spacecraft surface were calculated with a local flow inclination dependent method given by Daley[9]. A Knudsen number bridging function was used to combine free-molecular and continuum heat fluxes in the transitional flow regime.

The aerothermodynamic methods of SCARAB 1.0 proved to be not flexible enough for re-entry objects of arbitrary shape like satellites, while providing good results only for aerodynamically shaped objects like capsule or rocket noses. A new method was developed for SCARAB 1.5 and later. This method works more similar to the aerodynamic method, calculating local heat transfer coefficients (Stanton numbers) for each panel.

The laminar-turbulent transition is now neglected by this method. During the development of SCARAB 3.0, much effort was put into the development of turbulent extension with streamline tracing. Unfortunately, this attempt failed due to the complex arbitrarily shaped re-entry objects, which was also the reason to revise the original aerothermodynamic method of SCARAB 1.0.

$$\dot{Q}_{p,conv} = A_{p,us}\, St\, \rho_\infty V_\infty \cdot \left(0.5 V_\infty^2 - c_{p,air}\,(T_W - T_\infty)\right) \tag{15}$$

$$\dot{Q}_{conv} = 0.5\, \rho_\infty V_\infty^3 \int_{S_{us}} St\, dS_{us} - \rho_\infty V_\infty c_{p,air} \int_{S_{us}} St\,(T_W - T_\infty)\, dS_{us} \tag{16}$$

$A_{p,us}$	Unshadowed panel surface area
St	Local heat transfer coefficient (Stanton number) of the panel
$c_{p,air}$	Specific heat capacity of the air
$\dot{Q}_{conv}$	Total convective heat flux on the spacecraft

Free molecular flow:

$$St_{FM} = \frac{1}{2\sqrt{\pi}\, S_\infty^3} \cdot \left[\chi(S_n)\left(S_\infty^2 + \frac{\kappa}{\kappa-1} - \frac{(\kappa+1)\,T_W}{2\,(\kappa-1)\,T_\infty}\right) - 0.5\,\mathrm{e}^{-S_n^2}\right] \tag{17}$$

with $\kappa = 5/3$ for full accommodation of the molecule's translational energy and no accommodation of their internal energy.

Continuum flow (modified Lees [10] theory):

$$St_C = \frac{2.1}{\sqrt{Re_{\infty,0}}}\, f_C(\theta) \tag{18}$$

with:

$$Re_{\infty,0} = \frac{V_\infty \rho_\infty L_{ref}}{\mu(T_0)}$$

$$\cos\theta > 0: \quad f_C = 0.1 + 0.9\cos\theta$$
$$\cos\theta \le 0: \quad f_C = 0.1$$

$Re_{\infty,0}$	Modified Reynolds number
L_{ref}	Spacecraft reference length (same as for Knudsen number calculation)

Transitional regime (bridging function):

$$St = \frac{St_{FM}}{\sqrt{1 + (St_{FM}/St_C)^2}} \tag{19}$$

3.3. Shadow Analysis

All panels of the spacecraft geometry are subject to a shadow analysis because panels can be shadowed from the flow. Only the unshadowed surface fraction of each panel contributes to the aerodynamic and aerothermodynamic loads (see Eqs. 7, 8, 15, and 16). The shadow analysis of SCARAB is based on geometric area projections in flow direction. Flow expansion behind shadowing panels is neglected ($Ma_\infty, S_\infty \to \infty$).

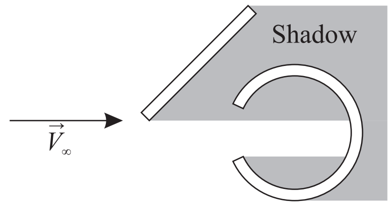

FIG. 3: Shadow Analysis Schematic

There are two types of shadowing. Leeward panels ($\cos\theta < 0$) are shadowed from the flow by themselves. Windward panels can be shadowed by other panels lying in front of them.

3.4. Panel Definition and Melting

The geometric primitives of SCARAB 1.0 defined only surface shells with zero wall thickness. The real wall thickness was only virtually specified by the user in order to facilitate the calculation of mass, center of mass, and moments of inertia of each primitive. Also the thermal analysis required the mass of each surface panel.

The aerodynamic and aerothermodynamic loads were only calculated for the outside surface of each panel. The back side surface (semi-transparent panels of the left cone in FIG. 4) was not considered by the analysis modules. Therefore, SCARAB 1.0 was only capable to analyze geometries with completely closed surfaces. In case of the left cone shown in FIG. 4, this meant that the geometry had to be closed by two circular discs, for example.

The problem of unconsidered back side surfaces reappeared though at later steps of the re-entry analysis when panels start to melt and holes in the surface are generated. If holes are present, the back side surfaces are no longer shadowed completely and must be taken into account by the aerodynamic and aerothermodynamic analysis. Also the exposed edges of panels around such holes with zero wall thickness do not represent the geometry correctly anymore.

In summary, it has to be concluded that SCARAB 1.0 could perform re-entry analyses only until the first melting of a surface panel. This limitation was resolved by SCARAB 1.5.

The most important improvement of SCARAB 1.5 was the introduction of volume panels (see FIG. 5). Each volume panel of a geometric primitive defines now not only one outside surface panel but up to eight: one front side panel (identical to the original surface panel), one back side panel (separated from the front side by the wall thickness), and up to six lateral panels (depending on the covering by neighbor panels).

Molten volume panels (incl. all surface panels) are automatically removed during the re-entry analysis. Newly exposed lateral surface panels are automatically generated if

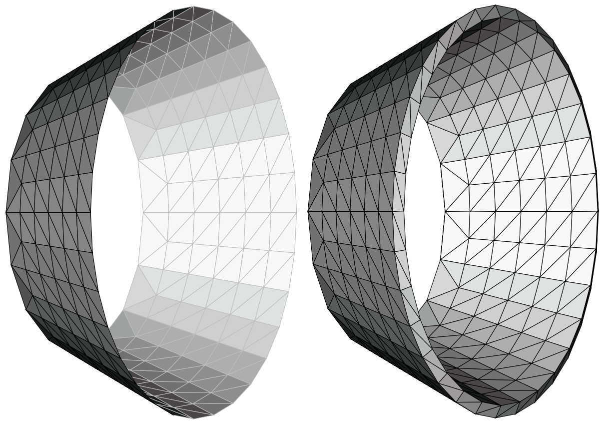

FIG. 4: Surface Panelization – SCARAB 1.0 (left) vs. SCARAB 1.5 and later (right)

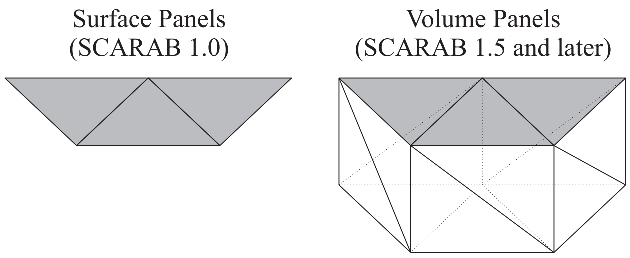

FIG. 5: Surface Panels vs. Volume Panels

neighbor panels have been removed due to melting. The exposure of formerly shadowed inside panels is correctly treated by the shadow analysis. All mass properties (i.e. total mass, center of mass, moments of inertia) are continuously updated based on current volume panel data.

The implementation of this SCARAB feature, the so-called pane-wise melting, was the major development step to make SCARAB applicable to real re-entry analysis scenarios.

4. IMPROVEMENTS FOR LAUNCHER

In addition to the total mass and size, the most significant difference between launcher stages and satellites is the presence of very large tanks containing a huge amount of propellant. The liquid and gaseous tank contents can be a multiple of the structural mass. At the time of re-entry residual tank contents can influence the dynamic and destruction behavior of the stage. This section will outline the tank specific analysis capabilities of SCARAB.

4.1. Tank Bursting

During re-entry, the aerothermodynamic loads are directly increasing the tank wall temperature. The tank content is also heated due to thermal conduction from the tank wall into the tank content (liquid and/or gaseous). This will finally lead to an evaporation of the liquid (if present). Throughout this heating process, the tank pressure p_t is increasing. In parallel, the temperature increase of the tank shell decreases the strength of the tank material, reducing the burst pressure p_b of the tank. The final consequence is the bursting of the tank if the tank pressure exceeds the burst pressure.

The first tank analysis method of SCARAB was already developed for SCARAB 1.5 as an external tool during the reentry analyses for ATV. This method was integrated completely into SCARAB 3.0.

The current tank analysis specifies tank contents (liquid and gaseous) as a mass point with uniform temperature inside of the tank shell. The tank heating process can be subdivided into three phases (if liquid is present):

1. Liquid/gas heating phase → pressure increase due to liquid expansion and gas heating
2. Liquid evaporation phase → pressure increase dominated by evaporation process, tank pressure equals evaporation pressure of the liquid ($p_t = p_v$)
3. Vapor/gas heating phase → pressure increase due to heating of gaseous tank contents

These phases are also illustrated in FIG. 6. For pure gas tanks, only the third phase is applicable.

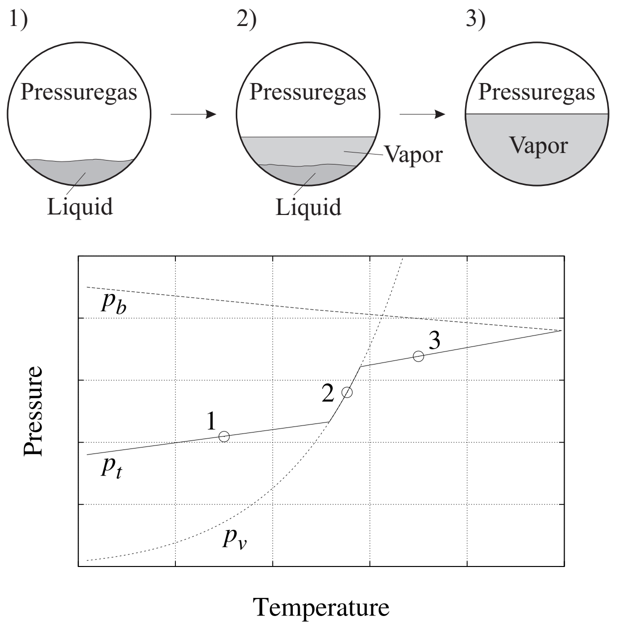

FIG. 6: Liquid Evaporation during Re-entry – Tank Pressure Increase and Bursting Pressure Decrease

The tank analysis of SCARAB 3.0 considers only liquid-gaseous phase transitions and vice-versa. SCARAB 3.1L will include all possible phase transitions for tank contents. Especially freezing and deposition (gas-to-solid) turned out to be relevant for the cryogenic propellants of the Ariane-5 EPC. FIG. 7 shows the simplified phase diagram that will be the basis for modeling three-phase material properties of tank contents in the SCARAB material database.

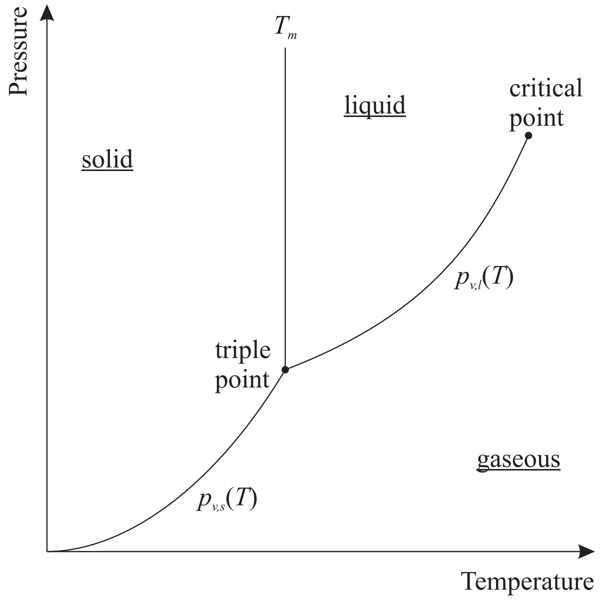

FIG. 7: Phase Diagram for Tank Contents (SCARAB 3.1L)

The decrease of the burst pressure is computed based on user-defined reference bursting conditions. A reference tank burst pressure $p_{b,ref}$ is specified for a reference temperature $T_{b,ref}$ (manufacturer data). These values are correlated with the decreasing ultimate tensile strength σ_{max} between $T_{b,ref}$ and the current maximum tank wall temperature $T_{tw,max}$ which corresponds to the weakest point of the tank shell:

$$p_b(T_{tw,max}) = p_{b,ref} \cdot \frac{\sigma_{max}(T_{tw,max})}{\sigma_{max}(T_{b,ref})} \qquad (20)$$

4.2. Tank Explosion

In SCARAB 3.0, a tank bursting event has no destructive consequences on the re-entry object. Only the tank contents are released, reducing the total mass of the spacecraft. However, the release of high energetic fuels into the high enthalpy flow environment during re-entry is likely to ignite such tank contents. This could possibly cause an explosion of the burst tank.

Fuel tank explosions and the corresponding fragmentation of the re-entry object will be treated by SCARAB 3.1L. A fragment generator based on the breakup model of NASA's EVOLVE 4.0[11] has been developed. If an explosion event is detected during re-entry, the re-entry object is destroyed completely. Explosion fragment properties like size and mass are randomly sampled according to the distribution functions of the breakup model. A shape identification algorithm determines the most likely simplified geometric shapes (i.e. spheres, boxes, cylinders) that are in line with the fragment parameters.

In a next step, all explosion fragments are subject to a re-entry analysis with SESAM (Spacecraft Entry Survival Analysis Module, SESAM[12]). SESAM is a fast, 3 degrees-of-freedom (no attitude computation, random tumbling assumed) re-entry analysis tool for simplified geometric objects. SESAM has the capability to analyze thousands of explosion fragments down to the ground within only a few seconds.

As for a standard SCARAB analysis, the final output of a SESAM analysis are number, size, mass, and impact velocity of all surviving fragments, as well as their impact locations. These data can be used to asses the risk for people on the ground to be hit or injured by surviving spacecraft fragments.

During the latest discussions for the development of SCARAB 3.1L it was proposed not to destroy the complete re-entry object into fragments according to the breakup model. Especially the complete breakup of components consisting of high strength materials (e.g. a rocket engine) is considered as rather unrealistic. Therefore, methods will be developed to exclude certain materials from the fragment generation process and follow-on SESAM analysis. These materials should be treated as intact SCARAB fragments.

4.3. Tank Sloshing

Sloshing of liquids is a complex effect depending on many parameters like tank shape, liquid properties, container movement, acceleration, etc.[13] For the use in the SCARAB 3.1L software, a simplified model had to be created which depends only on the acceleration vector of the spacecraft, the liquid volume and the tank shape. This model is based on the combination of three independent damped spring-mass systems which are oriented perpendicularly to each other and each one is parallel to one of the axes of the tank-fixed coordinate system. The equation of motion for such a system is given in Eq. 21.

$$\ddot{x}_i + 2 D_i\, \omega_i \dot{x}_i + \omega_i^2 x_i = 0 \qquad (21)$$

x_i	Spring elongation for system i w.r.t. tank-fixed coordinate system
D_i	Damping coefficient for system i
ω_i	Circular frequency for system i

For the calculation of the frequencies, a method developed by Leonard and Walton[14] is used. This method describes the determination of sloshing frequencies in rotational elliptic tanks. Three kinds of sloshing are distinguished depending on the acceleration vector acting on the liquid: horizontal, longitudinal, and transversal sloshing (see FIG. 8). The original equations are given in Eqs. 22–24.

$$\omega_h = \sqrt{\frac{g}{r_{free}} \varepsilon_n \tanh\left(\frac{h_{circ}}{r_{free}} \varepsilon_n\right)} \qquad (22)$$

$$\omega_l = \sqrt{\frac{g}{\alpha_{free}} k_{l,n} \tanh\left(\frac{h_{ell}}{\alpha_{free}} k_{l,n}\right)} \qquad (23)$$

$$\omega_t = \sqrt{\frac{g}{\alpha_{free}} k_{t,n} \tanh\left(\frac{h_{ell}}{\alpha_{free}} k_{t,n}\right)} \qquad (24)$$

ω_h	Horizontal frequency
ω_l	Longitudinal frequency
ω_t	Transverse frequency
g	Gravitational acceleration
r_{free}	Radius of circular free surface
α_{free}	Semi mayor axis of elliptical free surface
h	Liquid depth of the ellipsoidal tank
h_{circ}	Liquid depth in reference circular cylinder, $h_{circ} = f(h, r_{circ})$
h_{ell}	Liquid depth in reference elliptical cylinder, $h_{ell} = f(h, \alpha_{circ})$
ε_n	n^{th} root of first derivative of Bessel function of first order and first kind
$k_{l,n}, k_{t,n}$	Constant proportional to positive parametric zeros of the first derivatives of the Mathieu function
n	Sloshing mode

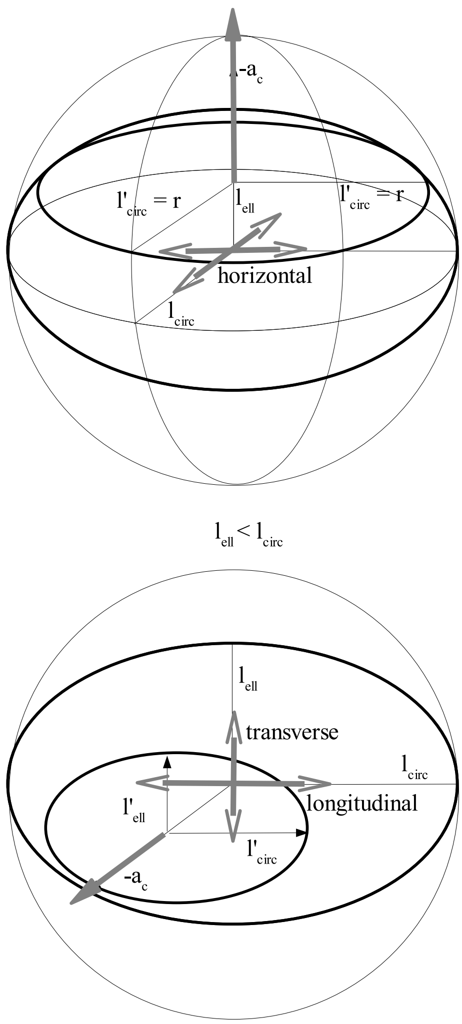

FIG. 8: Sloshing Directions: Horizontal, Longitudinal, and Transversal Sloshing

These equations needed to be modified for the use in SCARAB during re-entry. The constant gravitational acceleration is replaced by the actually acting acceleration vector of the spacecraft. Only the first sloshing mode is considered and a correction factor is introduced. The frequencies depend on the filling height, the acceleration and the eccentricity of the tank.

Due to the fact that only accelerations parallel to the main axes of the rotational ellipsoid were investigated by Leonard and Walton[14], a bridging method had to be found. Sloshing frequencies can be calculated based on one component of the acceleration vector for the two other directions. This yields six frequencies in total (two per direction). Weighted mean values are used for each direction, with the acceleration vector components as weighting factors.

In order to use this model, the real tank shape has to be transfered into an equivalent rotational elliptic tank. This is achieved by determining the maximum tank dimensions for each tank axis. The mean value of the two length values with the smallest difference is considered as the length of the two equal axes of the ellipsoid. The third axis has the length of the other main axis of the tank. The equivalent tank has to fulfill two conditions: the ratio of the two main axes has to be equal to the ratio of the original tank, and the equivalent tank has to have the same volume.

The position of the center of mass of the liquid at the beginning of a SCARAB simulation time interval is compared to the steady state position. This provides the displacement at the beginning of the time interval for each direction. The center of mass moves during the interval according to the oscillation equation (Eq. 21). The damping coefficients must be specified by the user. The steady state position of the center of mass is calculated under the assumption that the steady state surface will be oriented normal to the acceleration vector.

In SCARAB 3.0, liquid tank contents are modeled as fixed mass points located in the center of mass of each tank. In SCARAB 3.1L, these mass points can move. Therefore, also the spacecraft center of mass can move. This causes also changes of the moments of inertia. In SCARAB 3.0, the center of mass and the moments of inertia are only changed by fragmentations and panel melting. However, they are assumed to be constant during a time interval. Therefore, the $\dot{I}\,\vec{\omega}^B_{I,B}$ term in Eq. 3 could be neglected. This is not true anymore for SCARAB 3.1L due to the simulation of sloshing effects.

One test case for the sloshing module was a cylindrical tank with spherical endings. The re-entry started at 200 km altitude with a velocity of 7 km/s. The tank had a initial pitch rate of 60 deg/s. The tank was filled with about 37 m^3 of liquid hydrogen, with a mass of about 3 t. 5 kg of Helium were used as pressure gas. The tank had a total length of about 20 m. The diameter was about 5.4 m. FIGS. 9–12 show some SCARAB results with and without simulation of sloshing.

At the beginning of the re-entry, the centrifugal force is dominating. Gravitational and aerodynamic accelerations do not influence the tank content. Thus, the liquid is located at one end of the tank. At lower altitudes, when the aerodynamic forces on the spacecraft increase, the stable tank rotation is disturbed and the liquid starts to slosh causing a tumbling motion of the tank.

Due to the tumbling of the tank, the liquid center of mass moves into the direction of the center of the tank. This effect is also increased due to the beginning evaporation of the liquid hydrogen. The spacecraft center of mass also moves closer to the center (see FIG. 9). This has a large influence on the movement because the pitch rate is damped by this effect (see FIG. 10). The positive pitch rate is finally reduced to zero and afterward oscillates around zero with a high amplitude.

The other two rotation rates are shown in the FIGS. 11 and 12. They also increase much more than in the case without sloshing simulation. For the analyzed tank, the consideration of sloshing effects results in an earlier and much more pronounced tumbling motion.

Another interesting effect was that due to the different tank motion some panels of the sloshing tank got higher heat fluxes than without sloshing. Therefore, the bursting pressure was reached earlier. The sloshing tank burst at higher altitudes.

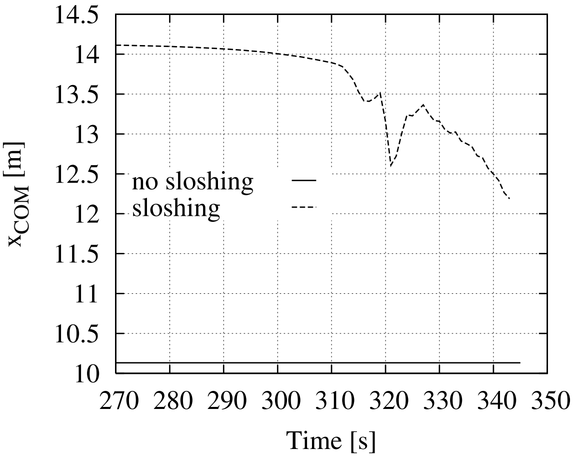

FIG. 9: Spacecraft Center of Mass (COM, length direction of the tank)

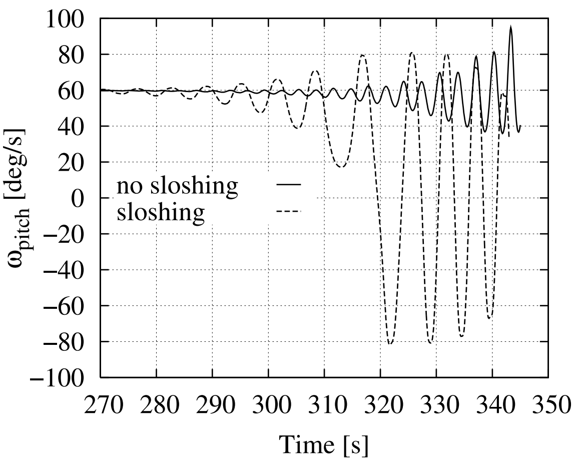

FIG. 10: Pitch Rate

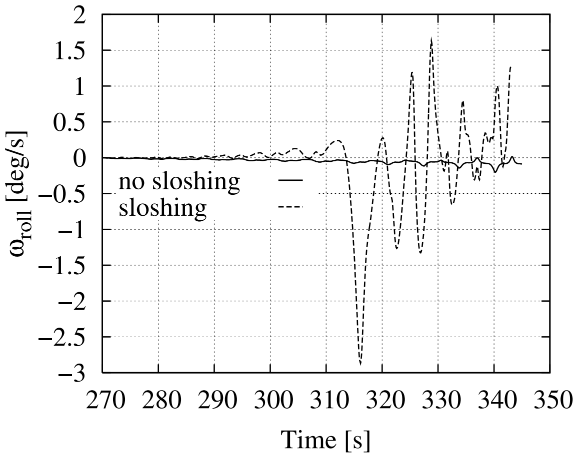

FIG. 11: Roll Rate

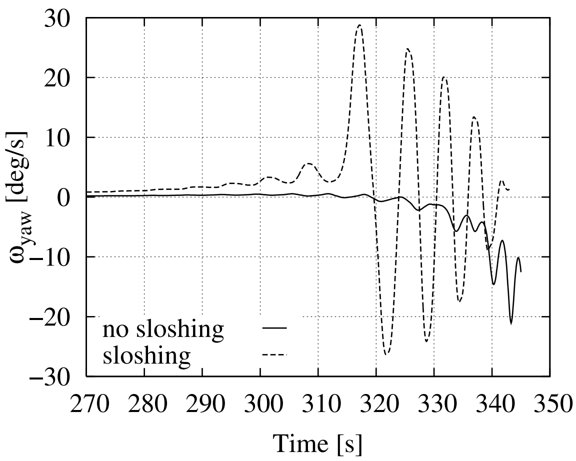

FIG. 12: Yaw Rate

5. SUMMARY AND CONCLUSIONS

SCARAB is a software tool for the numerical simulation of the destruction process of spacecraft re-entering the Earth's atmosphere. This paper has described the development history of SCARAB from its first release in 1997 to the latest development steps for the new SCARAB 3.1L which will provide dedicated analysis modules for the re-entry of launcher stages. The general analysis approach for the three basic tasks of a re-entry analysis – dynamic, thermal, and fragmentation analysis – has been outlined, and analysis methods for the calculation of aerodynamic and aerothermal loads have been presented. All these methods are based on triangularly panelized geometry definitions for the re-entry object. While surface panels with zero wall thickness were sufficient for the calculation of aerodynamic and aerothermal loads, the introduction of volume panels with the actual wall thickness was necessary to perform a complete destruction analysis on panel level. The essential development of the so-called panel-wise melting for SCARAB 1.5 brought the software to applicability for real space projects and the required risk assessments within such projects.

The latest re-entry analyses for the Ariane-5 program revealed special needs for the simulation of launcher specific effects. The major difference between launchers and satellites identified in this context is the presence of large tanks with a high amount of propellant inside. Therefore, the development of the new SCARAB 3.1L has been initiated in 2006. This version should be finalized by the end of 2008. This paper has described the implementation of three tank specific analysis capabilities: tank bursting, explosion, and sloshing. Especially the introduction of the simulation of liquid sloshing inside of tanks constitutes another major step for the improvement of SCARAB. Sloshing has a dominating effect on the dynamics of a re-entering launcher stage and thus also on the follow-on destruction process until the tank is damaged and the liquid is released.

REFERENCES

[1] B. Fritsche, G. Koppenwallner, et al. *Spacecraft Disintegration during Atmospheric Re-entry*. Executive Summary Report, ESOC Contract No. 11427/95/D/IM, Hypersonic Technology Göttingen, Katlenburg-Lindau, Germany, October 1997.

[2] B. Fritsche, G. Koppenwallner, et al. *Advanced Model for Spacecraft Disintegration during Atmospheric Re-entry*. Executive Summary Report, ESOC Contract No. 12804/98/D/IM, Hypersonic Technology Göttingen, Katlenburg-Lindau, Germany, April 2000.

[3] B. Fritsche, G. Koppenwallner, et al. *Uncontrolled Re-entry of Risk Objects*. Final Report, ESOC Contract No. 13946/99/D/CS, Hypersonic Technology Göttingen, Katlenburg-Lindau, Germany, 2002.

[4] B. Fritsche, H. Klinkrad, et al. Spacecraft Disintigration during Uncontrolled Atmospheric Re-entry. In *Acta Astronautica*, 47(2–9):pp. 513–522, 2000.

[5] T. Lips, B. Fritsche, et al. *Upgrade of SCARAB Capabilities for Enhanced Performance and Portability*. Executive Summary Report, ESOC Contract No. 15756/01/D/HK, Hypersonic Technology Göttingen, Katlenburg-Lindau, Germany, November 2005.

[6] T. Lips, B. Fritsche, et al. Ariane-5 EPC Re-entry – A Comparison of Observations and SCARAB Simulation Results. To be published in the *Proceedings of the Second IAASS Conference*, Chicago, USA, May 14–16, 2007.

[7] R. W. Detra, N. H. Kemp, and F. R. Riddell. Addendum to 'Heat Transfer to Satellite Vehicles Re-entering the Atmosphere'. In *Jet Propulsion*, 27(12):pp. 1256–1257, December 1957.

[8] R. W. Detra and H. Hidalgo. Generalized Heat Transfer Formulae and Graphs for Nose Cone Re-entry into the Atmosphere. In *American Rocket Society*, 31(3):p. 318, March 1961.

[9] S. Daley. *FRENEW Version 3.0: Program Description and User Guide*. FGE Report TN 101/94, Fluid Gravity Engineering Ltd., Liphook, Hampshire, United Kingdom, August 1994.

[10] L. Lees. Laminar Heat Transfer over Blunt Nosed Bodies at Hypersonic Speed. In *Jet Propulsion*, 26(4):pp. 259–269, 1956.

[11] N. L. Johnson, P. H. Krisko, et al. NASA's New Breakup Model of EVOLVE 4.0. In *Advances in Space Research*, 28(9):pp. 1377–1384, 2001.

[12] T. Lips, B. Fritsche, and G. Koppenwallner. *SESAM Final Report – Development of a Re-entry Risk Assessment Tool for the DRAMA Software*. Final Report, ESOC Contract No. 16642/02/D/HK(SC), Hypersonic Technology Göttingen, Katlenburg-Lindau, Germany, September 2004.

[13] H. N. Abramson (Editor). *The Dynamic Behavior of Liquids in Moving Containers*. NASA, Washington, D.C., USA, 1966.

[14] H. W. Leonard and W. C. Walton, Jr. *An Investigation of the Natural Frequencies and Mode Shapes of Liquids in Oblate Spheroidal Tanks*. Technical Note D-904, NASA, Washington, D.C., USA, 1961.